

THE QUANTITATIVE ANALYSIS OF GASEOUS MIXTURES
VIA MICROWAVE LINE INTENSITY MEASUREMENTS

A THESIS

Presented to

The Faculty of the Division of Graduate Studies

By

Ralph Alan Patterson


In Partial Fulfillment
of the Requirements for the Degree
Master of Science in Physics

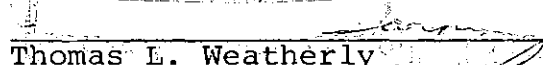
Georgia Institute of Technology

August, 1976

THE QUANTITATIVE ANALYSIS OF GASEOUS MIXTURES
VIA MICROWAVE LINE INTENSITY MEASUREMENTS

Approved:


Joel Q. Williams, Chairman


Thomas L. Weatherly


Michael J. Matteson

Date approved by Chairman AUG 24 1976

ACKNOWLEDGMENTS

I would like to thank Dr. Michael J. Matteson and the Georgia Institute of Technology Air Quality Control Committee for their financial support which made my graduate study possible. I would like to acknowledge Dr. Edwin J. Schiebner for it was he that helped me settle on this field of research. To Dr. Joel Q. Williams, Thesis Adviser, and Dr. Thomas L. Weatherly I am deeply indebted for their patience, their time, and their guidance. Last of all my heartfelt thanks go to Mr. and Mrs. Jack O. Patterson, Sr. and my entire family for their undying support.

TABLE OF CONTENTS

	Page
ACKNOWLEDGMENTS	ii
LIST OF TABLES	iv
LIST OF ILLUSTRATIONS	v
SUMMARY	vi
Chapter	
I. INTRODUCTION	1
Advantages of MRR Spectroscopy	
Limitations of MRR Spectroscopy	
Harrington's New Absorption Coefficient	
Γ in the Laboratory	
II. EXPERIMENTAL APPARATUS	14
The Microwave Spectrometer	
Gas Handling System	
Crystal Current Control Device	
III. CALIBRATION PROCEDURE	33
Sample Preparation	
MRR Line Intensity Measurement	
IV. THE CALIBRATION CURVE	39
V. CONCLUSIONS AND RECOMMENDATIONS	46
APPENDIX A	49
APPENDIX B	51
BIBLIOGRAPHY	59

LIST OF TABLES

Table	Page
1. Pollutants Measurable Using a Typical MRR Spectrometer (Can Detect an Absorption Coefficient Equal to 10^{-9} cm^{-1})	6
2. Experimental Data Supporting the Effectiveness of the Crystal Current Control Device	30
3. Slope Intercept Data for the Calibration Curve and the Four Test Sequences	42
4. Test Sequence One	53
5. Test Sequence Two	54
6. Test Sequence Three	55
7. Test Sequence Four	56

LIST OF ILLUSTRATIONS

Figure	Page
1. Microwave Spectrometer Components	15
2. Good 85 KHz Preamp	18
3. Gas Handling System	19
4. The HP X421A Crystal Detector	22
5. Crystal Detector Waveforms for Samples Having Different Partial Pressures of Test Gas $P_B > P_A$	23
6. Crystal Current Control Device	26
7. Crystal Input Waveform as a Result of External Applied Voltage	28
8. Crystal Detector Waveforms for SO_2 Using the Crystal Current Control Device	31
9. Signal Stabilizes Within Fifteen Minutes	36
10. The Calibration Curve	41

SUMMARY

The measurement of partial pressures of gases using a conventional microwave spectrometer was investigated. An electronic device was employed to maintain a constant crystal detector gain. A technique for calibrating the microwave spectrometer by relating the amplitude of a microwave rotational resonance (MRR) line to the partial pressure of the gas in the absorption cell is presented. A calibration curve was constructed for partial pressures of sulfur dioxide in the range of one to thirty millitorr in a sample having a total pressure of 100 millitorr. The curve was found to be linear within an error of 7.6 per cent as determined by a least squares fit computer program. The minimum detectable change in the amount of sulfur dioxide was calculated to be 0.1 millitorr. The data indicated some alteration of the sample with time, and possible mechanisms for explaining this are discussed.

CHAPTER I

INTRODUCTION

The deterioration of the environment as a result of unchecked industrial, commercial, and transportation related emissions and subsequent air pollution episodes in the last two decades precipitated a world-wide concern for the quality of the air in which we live. Within the national scope this concern was climaxed by the passage of the Clean Air Act in 1970 establishing ambient standards for the major pollutants as well as emission standards for the sources of the pollutants (1). Concurrent with the passage of the Clean Air Act arose the need for systems and techniques capable of monitoring a wide variety of gaseous pollutants in the highly complex ambient and industrial atmospheres. Systems utilizing wet chemical techniques were initially prominent, but there exists an ever-increasing trend toward systems using physical methods. One such physical method presently in developmental stages utilizes microwave rotational resonance (MRR) spectroscopy (2,3,4,5,6,7,8). MRR spectroscopy is generally used in the determination of molecular structure and related constants.

Advantages of MRR Spectroscopy

Certain characteristics of MRR spectroscopy make it

highly desirable for use in trace gas monitoring instrumentation. They are as follows:

(1) The microwave region of the electromagnetic spectrum exhibits a tremendous information carrying capability. For the 10,000 to 50,000 MHz region and a typical line-width of one MHz there is room for 40,000 resolved lines.

(2) Microwave frequencies are conducive to the use of extremely high resolution electronic techniques.

(3) The MRR spectrum is a highly characteristic property of the molecule that is determined uniquely by the three associated moments of inertia (9). A molecule can thus be unambiguously distinguished from all others via its MRR spectrum. Furthermore, it has been indicated that a single MRR line identifies the absorbing gas with ninety-five percent certainty (10).

(4) For many common pollutants the fractional amount of microwave power absorbed per unit path length, the absorption coefficient, is as large as 10^{-5} cm^{-1} for at least one MRR line. It is presently possible to construct a microwave spectrometer capable of detecting an absorption coefficient as small as 10^{-12} cm^{-1} so it is reasonable that fractional abundances of 100 parts per billion of many common pollutants are detectable (11).

(5) Due to the small energies involved power requirements are minimal.

(6) Sampling problems are minimized since in most

cases only 10^{-12} to 10^{-6} moles of sample are required.

(7) The response time of the microwave spectrometer is usually less than one minute so MRR spectroscopy is well suited for continuous monitoring.

(8) Since the line frequencies in the MRR spectrum of a gas are not affected by the presence of other gases, the capability exists for monitoring several components of a multicomponent mixture with a minimum of interference.

Limitations of MRR Spectroscopy

Fundamental Limitations

Certain fundamental properties of MRR spectroscopy limit its applicability to trace gas monitoring. Consider the Van Vleck-Weisscoff equation (12) for the fractional loss of microwave power per unit path length due to molecular absorption in equation (1).

$$\gamma(\nu) = \frac{8\pi^2}{3ch}(n_0 - n_1) |\mu_{01}|^2 \frac{\nu(\Delta\nu)}{(\nu - \nu_0)^2 + (\Delta\nu)^2} \text{ cm}^{-1} \quad (1)$$

Here $\gamma(\nu)$ is the absorption coefficient, ν is the radiation frequency, ν_0 is the transition frequency, $\Delta\nu$ is the line-width or $\frac{1}{2\pi\tau}$ where τ is the time between collisions that broaden the line, $|\mu_{01}|$ denotes the transition dipole matrix element connecting the two states involved, and n_0 and n_1 are the populations per unit volume of the ground and excited states respectively. The dipole matrix term arises because

of the nature of the microwave transition. The absorption of microwave energy by a molecule is a result of the interaction of the microwave electromagnetic field and the electric dipole moment of the molecule. Hence in order to exhibit an MRR spectrum the molecule must have an electric dipole moment. Ninety percent of the common pollutants do possess a dipole moment, and MRR spectra of most of these have been observed and cataloged. This is very important as it is necessary to absolutely identify the transition of the gas to be analyzed.

Note that in equation (1) the absorption coefficient is directly proportional to the difference in the populations of the two states involved in the transition. As a result of the very close spacing of rotational energy levels these differences are very small. Conversion of this population difference to the concentration or partial pressure of the absorbing gas requires knowledge of the partition function, the isotopic distribution, and the isomeric distribution of the absorber. These are indeed difficult to obtain.

The linewidth of an MRR line is directly proportional to the pressure of the sample gas. To assure the highest degree of specificity high vacuum techniques must be employed. Due to intermolecular interactions the MRR spectra of molecules having more than twelve atoms are extremely dense and complex so that in most cases the transitions have not been identified or cataloged. Fortunately most common pollutants

are of the smaller variety.

In summary, MRR spectroscopy is applicable to molecules in the gaseous state at low pressures. They must possess an electric dipole moment and consist of less than about twelve atoms. Some gases may have MRR spectra, but if the absorption coefficients are not large enough fractional abundances common to pollutants may not be measurable without selectively enhancing the concentration of the pollutant as is done most notably in gas chromatography. Some pollutants measurable by MRR spectroscopy are listed in Table 1 along with typical concentrations found in the atmosphere and concentrations measurable utilizing a spectrometer with average sensitivity.

Inseparability of N and τ

Though the above considerations somewhat limit the applicability of MRR spectroscopy they do not represent the impediment responsible for the slow development of this powerful analytical tool. Early attempts to deduce gaseous concentrations involved either the comparison of the spectrometer response for samples of unknown composition to that for samples of known composition or the absolute measurement of the integrated line intensity. The integrated line intensity is defined as the integral of the absorption coefficient over all frequencies (9), that is

$$\int_0^{\infty} \gamma(\nu) d\nu = \frac{8\pi^2}{3ch} (n_0 - n_1) |\mu_{01}|^2 \nu_0. \quad (2)$$

Table 1. Pollutants Measurable Using a Typical MRR Spectrometer (Can Detect an Absorption Coefficient Equal to 10^{-9} cm^{-1})

Pollutant	Typical Concentration	Measurable Concentration
CO	5-100 ppm	10 ppm
NH ₃	5-10 ppb	1 ppm
O ₃	0.1-0.2 ppm	--
HCHO	0.4-1 ppm	1 ppm
SO ₂	0.2-2 ppm	50 ppm
NO _x	0.01-0.5 ppm	--
acrolin	--	--

Assuming that the states are in thermodynamic equilibrium, then one has

$$(n_0 - n_1) \approx n_0 \frac{h\nu_0}{\kappa T} = fN \frac{h\nu_0}{\kappa T} \quad (3)$$

where κ is Boltzmann's constant, T is the temperature in degrees Kelvin, f is the fraction of the absorbing gas in the ground state of the transition, and N is the concentration of the absorbing gas. Combining (2) and (3) we have

$$\int_0^{\infty} \gamma(\nu) d\nu = \frac{8\pi^2 fN}{3c\kappa T} |\mu_{01}|^2 \nu_0^2$$

which one can write as

$$\int_0^{\infty} \gamma(\nu) d\nu = \gamma_{\max} \Delta\nu = \frac{8\pi^2 fN}{3c\kappa T} |\mu_{01}|^2 \nu_0^2 \quad (4)$$

where γ_{\max} is the absorption coefficient at the frequency for peak absorption. If both the maximum MRR line intensity and the MRR linewidth are measured, the absorber concentration can be deduced therefrom. The problem arises in the interpretation of the linewidth $\Delta\nu$. In a mixture of m gases at constant total pressure we have

$$\Delta\nu = \frac{1}{2\pi\tau} = \frac{1}{2\pi} \sum_{k=1}^m \frac{1}{\tau_{1k}} = \frac{1}{2\pi} \sum_{k=1}^m (Dx_k \nu_{1k}^{\sigma} 1k) \quad (5)$$

where τ is the time between collisions that broaden the line, τ_{1k} is the broadening time as a result of collisions with the k^{th} constituent, D is the total molecular density, x_k is the fractional abundance of the k^{th} constituent gas, v_{1k} is the relative velocity between the absorber and the k^{th} constituent gas, and σ_{1k} is the broadening cross-section for the absorber- k^{th} constituent collision (13). If all the τ_{1k} 's in equation (5) are equal, the maximum absorption coefficient is directly proportional to the absorber concentration. The fact is that in general the τ_{1k} 's are not all equal and hence the maximum absorption coefficient can be related to the absorber concentration only if all of the parameters in equation (5) are known. Rearranging equation (4) and noting that $\Delta\nu = \frac{1}{2\pi\tau}$ for samples of constant total pressure, we have

$$\gamma_{\text{max}} = \frac{16\pi^3 f |\mu_{01}|^2 \nu_0^2}{3ckT} (N\tau).$$

The maximum absorption coefficient is directly proportional to the product of N and τ and without the information contained in equation (5) one cannot relate the concentration N of the absorbing gas to the MRR spectrometer response.

The Power Saturation Effect

In the past another severe limitation to the application of MRR spectroscopy to the quantitative chemical analysis of gases was the power saturation effect. One observes

that as the microwave power through a gas is increased the MRR line peak intensity increases, goes through a broad maximum, decreases, and finally vanishes altogether. Upon inspection of equation (1) it is seen that the absorption coefficient is directly proportional to the difference in populations of the two states involved in the transition. For very low power levels this population difference is determined primarily by thermal considerations. In this so called Beer's law region of thermodynamic equilibrium the concentration of the absorbing gas is directly proportional to the population difference (refer to equation (3)) and thus to the absorption coefficient. For higher power levels the populations of the states are determined by thermal processes and also by absorption and stimulated emission induced by the microwave field. The probabilities for absorption and stimulated emission are equal, but the population of the ground state is greater. The net result is a decrease in the difference in the populations for the two states and the observed decrease in the absorption coefficient with increasing power. For high power levels the absorption coefficient is

$$\gamma_S(\nu) = \frac{n_0 (h\nu_0)^2}{\kappa T^2} \left[\frac{K}{1 + KP_0} \right] \quad (6)$$

where K is the saturation coefficient defined by the following equation:

$$K = \frac{16\pi^3 |\mu_{01}|^2 t\tau}{3ch^2}. \quad (7)$$

The incident microwave power level P_0 is assumed to be uniform throughout the absorption cell, and t is the time between collisions that relax the excited state (14). The dependence of the peak absorption on the microwave power level under high power conditions influenced early investigators to work in the Beer's law region using minimum power levels and consequently conditions of minimum sensitivity. Only molecular species with large absorption coefficients were investigated.

Harrington's New Absorption Coefficient

In a series of papers published in the Journal of Chemical Physics (15, 16), Howard W. Harrington has presented a new theory which allows the separation of N and τ and establishes the linearity of the MRR line peak intensity as a function of absorber concentration under conditions of power saturation. The theory is based on a new absorption coefficient Γ defined as the old $\gamma(\nu_0)$ times the square root of the incident microwave power, P_0 . From the definition we have

$$\Gamma = \frac{\Delta P_g}{LP_0}$$

where ΔP_g is the change in the microwave power as a result of

absorption by a gas in the path length L , and Γ is given by

$$\Gamma = \gamma P_0^{\frac{1}{2}} = \frac{\Delta P_g}{L P_0^{\frac{1}{2}}} \quad (8)$$

Combining equations (6) and (8) we have

$$\begin{aligned} \Gamma(\nu_0) &= \frac{n_0 (h\nu_0)^2}{\kappa T t} \left[\frac{K P_0^{\frac{1}{2}}}{1 + K P_0} \right] \\ &= \frac{n_0 (h\nu_0)^2}{\kappa T t} K^{\frac{1}{2}} \left[\frac{(K P_0)^{\frac{1}{2}}}{1 + K P_0} \right]. \end{aligned} \quad (9)$$

The term in the brackets is a dimensionless function of the microwave power and the saturation coefficient. Considering the definition of K in equation (7), if each collision that broadens the line also relaxes the excited state then $t = \tau$, and the problem of inseparability of N and τ is eliminated. The validity of this assumption is discussed elsewhere (15). Rewriting equation (9) in the fashion of Harrington we have

$$\begin{aligned} \Gamma &= \eta \phi(K P_0) \\ \eta &= \left(\frac{16\pi^3}{3c} \right)^{\frac{1}{2}} \frac{|\mu_{01}|}{\kappa T} n_0 \end{aligned} \quad (10)$$

$$\phi(K P_0) = \frac{(K P_0)^{\frac{1}{2}}}{1 + K P_0} \cdot$$

Then Γ is a product of a term η containing only molecular variables times ϕ , a function of KP_0 , which contains molecular variables and the microwave power density distribution in the sample. According to equation (1), for a particular value of KP_0 , i.e., a particular value of $\phi(KP_0)$, Γ is directly proportional to absorber concentration. The factorability of Γ is not peculiar to the uniform field case. For derivations of the power density distribution functions for lossless and lossy waveguides see references (17) and (18).

Γ in the Laboratory

Let us now examine the experimental consequences of requiring the constancy of KP_0 . Let

$$KP_0 = R = \text{constant.}$$

Recalling the definition of K in equation (7) and assuming $t = \tau$ we have

$$P_0^* = R \frac{3ch}{16\pi^3 |\mu_{01}|^2} \left(\frac{1}{\tau}\right)^2 \quad (11)$$

where P_0^* is the microwave power required to maintain the constancy of KP_0 . Combining equations (5) and (11) yields

$$P_0^* = R \frac{3ch^2}{16\pi^3 |\mu_{01}|^2} \left[\sum_{k=1}^m D_{x_k} v_{1k} \sigma_{1k} \right]^2 \quad (12)$$

It is evident that P_O^* is a complicated function of the relative concentrations of the constituent gases. To evaluate P_O^* for a given R and sample one must know all of the parameters expressed in equation (12) for the given sample. Since in general these are not known, P_O^* cannot be evaluated from equation (12). However, it is possible to keep $\phi(KP_O)$ constant experimentally. Note that in equation (10) $\phi(KP_O)$ is the only term having any power dependence, so that the maximum spectrometer response for a particular sample corresponds to the maximum of $\phi(KP_O)$. By adjusting the incident microwave power to maximize the absorption for all samples one maintains a constant microwave power density distribution function equal to $\phi_{\max}(KP_O)$.

If the detection system of the spectrometer is linear the maximum observed MRR line peak intensity is directly proportional to the absorption coefficient Γ and thus to absorber concentration (19). It is the purpose of this research to confirm this linearity and to develop a technique by which the conventional Stark-modulation microwave spectrometer can be calibrated to yield partial pressures of gases in mixtures. A calibration curve for sulfur dioxide will be constructed, and the minimum change in the amount of sulfur dioxide this instrument can detect will be determined.

CHAPTER II

EXPERIMENTAL APPARATUS

The experimental apparatus utilized in this research is a conventional Stark-modulation microwave spectrometer system with one alteration. In order to maintain a constant direct crystal current in the detector under various power conditions on the crystal an electronic device is employed that approximates the microwave bridge arrangement used by other investigators. The operation of this device and the degree of this approximation are discussed in the last section of this chapter. The microwave spectrometer and the accompanying gas handling system are described first.

The Microwave Spectrometer

As depicted in Figure 1 the spectrometer system is the conventional Stark-modulation microwave spectrometer. The source of microwave radiation is a Varian X-13 reflex klystron employing a Hewlett Packard (HP) Model 716B power supply. The HP power supply is operated in the external sweep mode, the sweep being furnished by a sawtooth generator. To keep reflected radiation from reaching the klystron a De Morray Bonardi DBG-480 isolator is positioned immediately after the klystron. The source power is regulated via an HP Model X375A, 0-20 dB, variable attenuator. In order to monitor

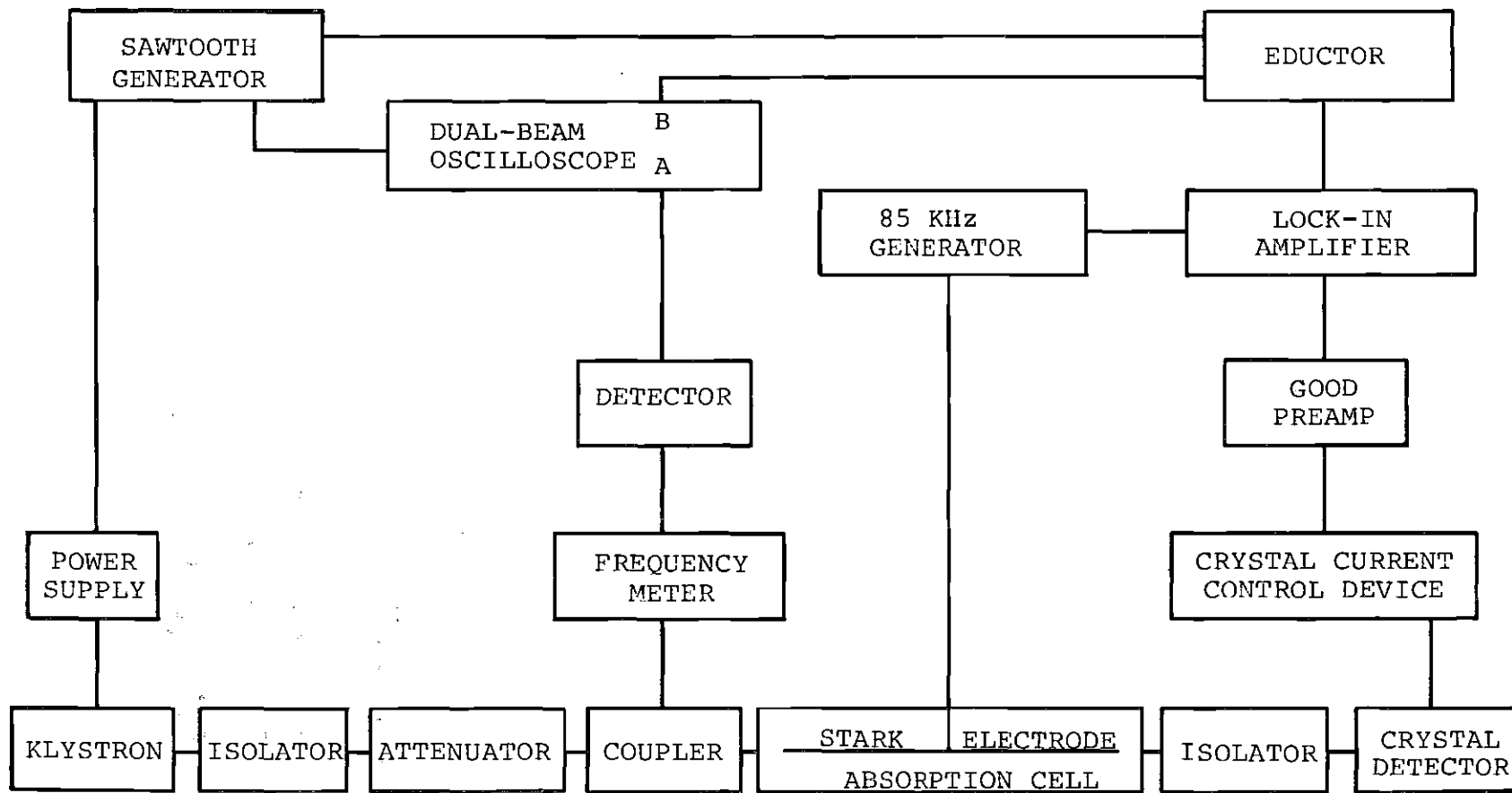


Figure 1. Microwave Spectrometer Components

the frequency of absorption and its position with respect to the mode of the klystron, an HP Model X752C, 10dB, directional coupler is used to couple some of the radiation through an HP X421A crystal detector whose output is displayed on channel A of an HP 132A dual beam oscilloscope. The horizontal sweep of the oscilloscope is furnished by the sawtooth generator mentioned above.

The absorption cell depicted in Figure 1 is constructed of copper rectangular X-band waveguide enclosed at both ends by mylar windows pressed between two waveguide flanges and sealed with beeswax and rosin. The cell is fitted with a Stark electrode of 0.021 inch copper sheet running the full length of the cell parallel to the broad face, supported and centered on both sides by teflon strips. The Stark voltage is applied to this electrode by an Industrial Components Incorporated 85 kHz square wave generator. At each end of the absorption cell are slits for the introduction and removal of samples.

Microwave radiation traversing the total length of the cell is guided through a Bomac Laboratories type BLF-304 isolator to an HP X421A crystal detector. The isolator is incorporated to prevent radiation reflected from the crystal detector from reentering the cell. The crystal detector current is then separated into its AC and DC components by the crystal current control device discussed later in this chapter. The AC component then becomes the input to an 85

kHz preamp described by Good (20) and shown schematically in Figure 2. This amplifier rejects signals outside of a narrow band of frequencies around 85 kHz. The resulting signal is then detected and amplified via a Princeton Applied Research (PAR) Model HR-8 lock-in amplifier using a type A preamp. The signal to noise ratio of the PAR output is not adequate for very small amounts of test gas, so a PAR Model TDH-9 waveform Educator is also used. This unit effectively picks the signal out of the noise by averaging a large number of sweeps. It also adds an additional gain factor to the overall detection system. The Educator sweep is initiated by a negative pulse from the sawtooth sweep generator. The Educator output is displayed on channel B of the HP dual beam oscilloscope.

Gas Handling System

The basic components of the gas handling system are depicted in Figure 3. A glasswork system is connected to the Stark cell via a kovar seal and copper tubing at the source end of the cell, and an all metal system is connected to the detection end of the Stark cell. The all metal system allows the introduction of the sample gases into the cell from commercial lecture bottles. Cell pumping is achieved by a Welch Duo-Seal Model 1405 mechanical fore pump and a Consolidated Vacuum type VMF-21 oil diffusion pump. All pumping in this work is done through a liquid nitrogen trap incorporated in

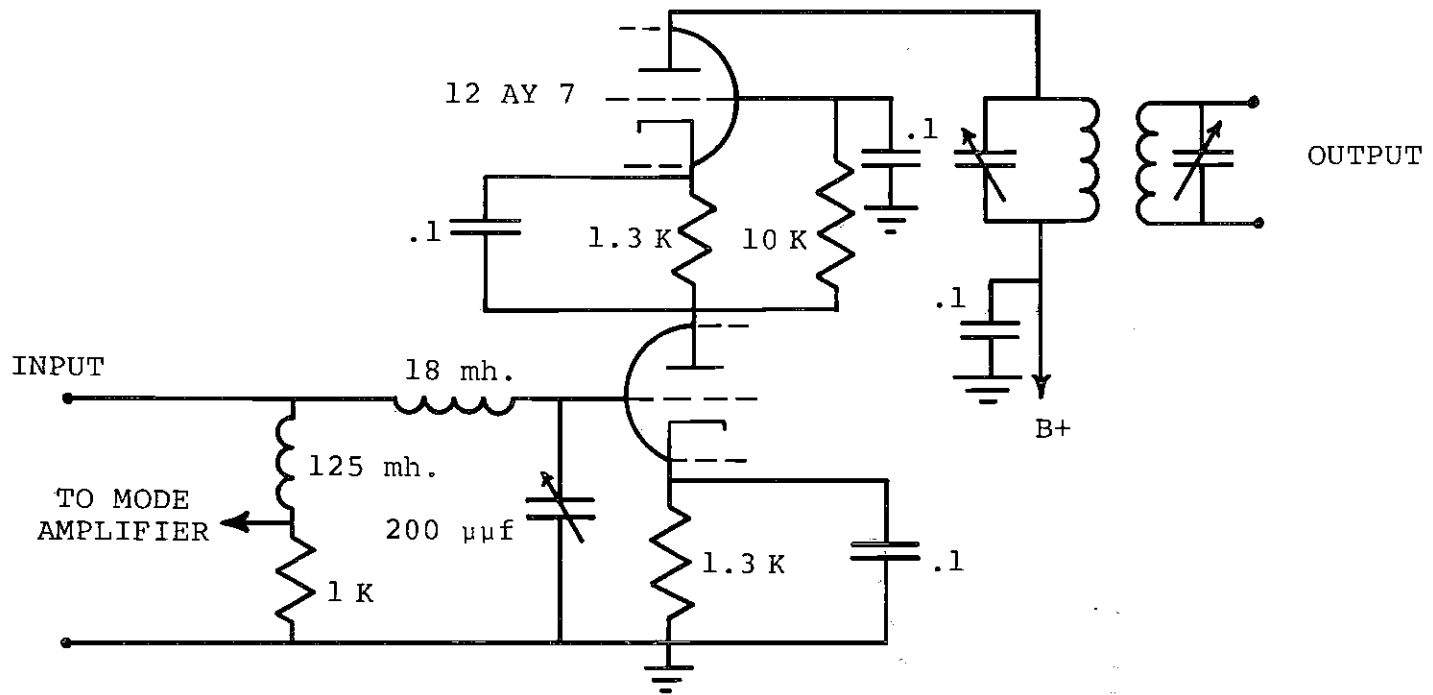


Figure 2. Good 85 KHz Preamp

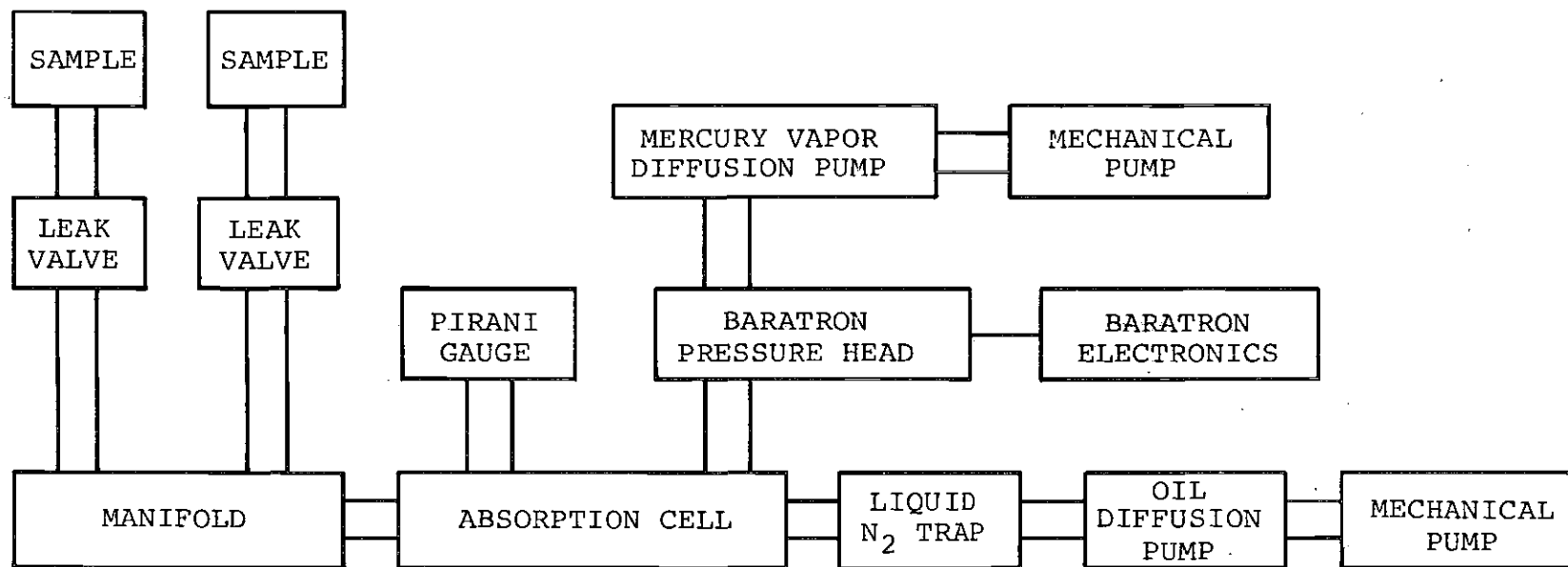


Figure 3. Gas Handling System

the glasswork. System pressure measurements are made roughly by an Distillation Products type PG-1A Pirani guage and precisely by an MKS Instruments type 77H-1 Baratron pressure meter using a one millimeter pressure head. Reference port vacuum is maintained by an Edwards High Vacuum Speedivac oil diffusion pump and liquid nitrogen trap all backed by a Welch Duo-Seal Model 1405 mechanical pump.

A sample gas inletting system allows the introduction of two gases in very small quantities into the cell from lecture bottles of gas at very high pressures. This is achieved via two Granville Phillips Co. series 203 leak valves which are connected on the high pressure side to the gas lecture bottles with quarter inch stainless steel tubing and Swagelok connectors. The low pressure side of each leak valve is then coupled to a small Varian flange manifold having three parts, one of which is connected to the Stark cell with kovar seals and glass tubing. The manifold and valves are mounted on an aluminum plate which, along with the lecture bottles of gas, is supported by a tubular superstructure. Linde gases used in this research are anhydrous, 99.9% minimum purity CGA-660 sulfur dioxide and prepurified 99.998% minimum purity CGA-580 nitrogen (21).

Crystal Current Control Device

Before discussing the crystal current control device it is necessary to discuss the operation of the crystal de-

detector. A schematic diagram of the HP X421A crystal detector is shown in Figure 4 (22). The e in Figure 4 represents the sinusoidal voltage induced in the crystal detector probe in the waveguide by the microwave radiation. This e is amplitude modulated at the Stark modulation frequency due to absorption by the gas when the Stark field is off. The change in e resulting from absorption is directly proportional to Γ (23). As discussed in Chapter I, Γ is directly proportional to absorber concentration provided that the microwave power density distribution function is kept constant.

Consider two samples of gas, A and B, at the same total pressure but differing in concentration of the absorbing gas such that the concentration in A is less than that in B, and suppose that the power required to maximize the MRR line for sample A is greater than that for B. It is informative to consider the waveforms associated with the crystal for each of these cases as shown in Figure 5. In the figure the solid waveforms are those at the microwave frequency present during the time the Stark voltage is on and the dashed waveforms are those present when the Stark voltage is off. The magnitudes of Δe and Δi are exaggerated to show clearly their relative sizes. The crystal output current waveforms i are shown to the right of the crystal response curves. Because of the capacitor C_L the voltage across the load resistor R_L is smoothed out and is equal to $\bar{i}R_L$ during

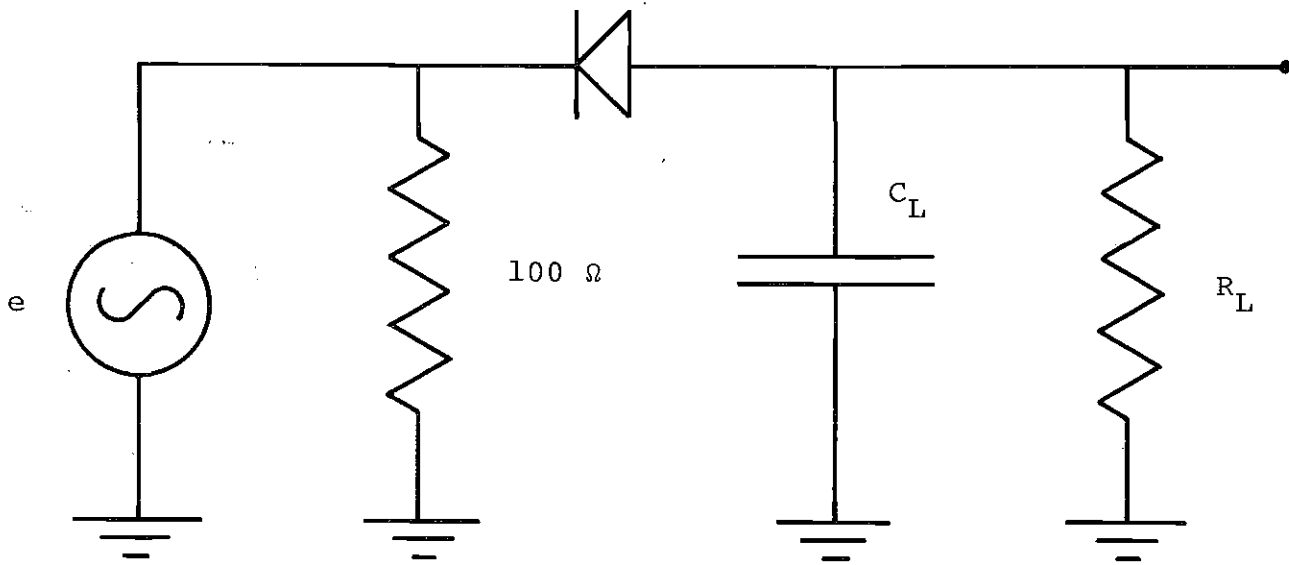


Figure 4. The HP X421A Crystal Detector

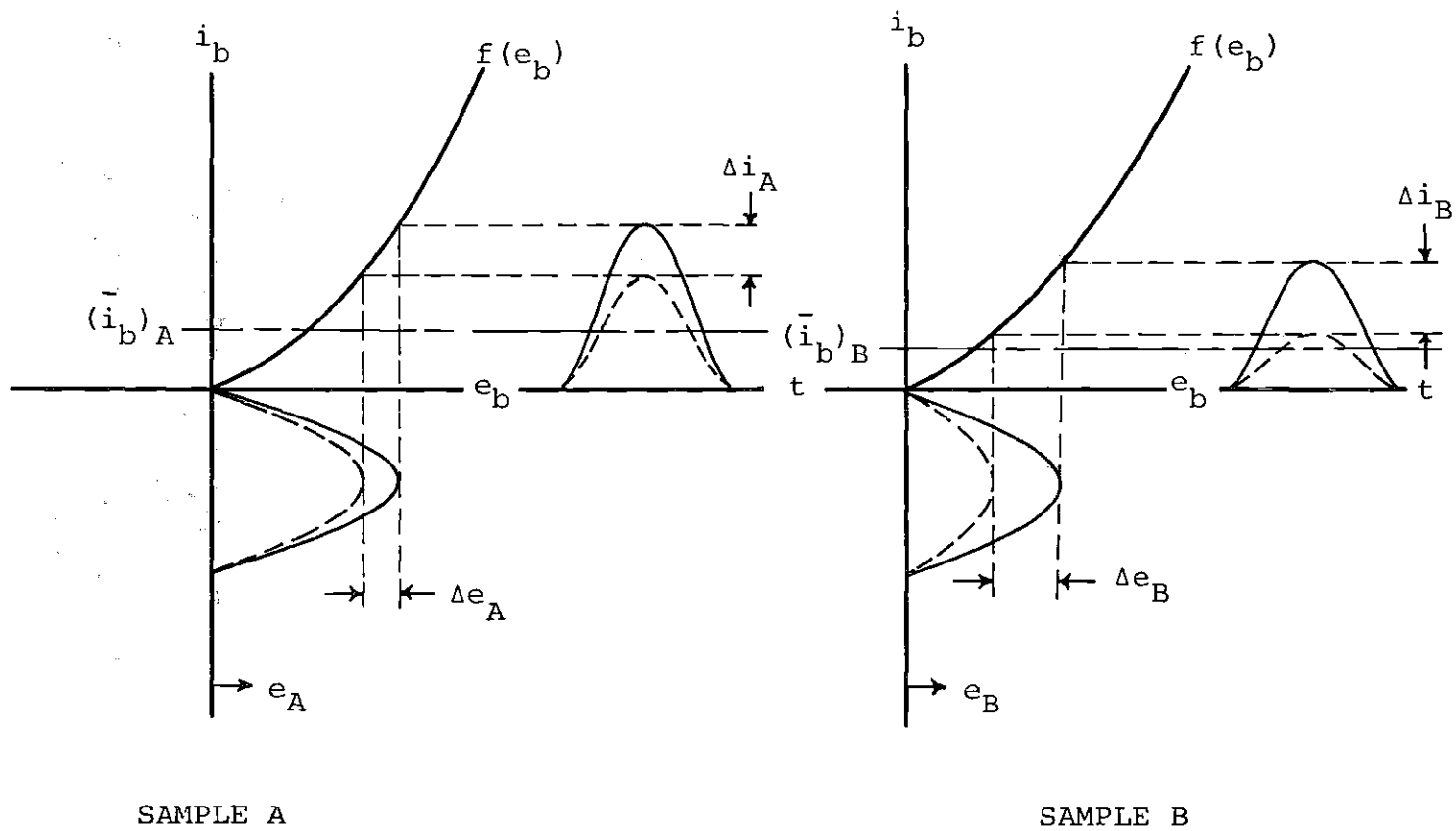


Figure 5. Crystal Detector Waveforms for Samples Having Different Partial Pressures of Test Gas $P_B > P_A$

the Stark-field-on period and $(\bar{i}-\Delta\bar{i})R_L$ during the Stark-field-off portion of the period. This voltage becomes the input to the Good preamp. Note that the voltage across R_L is a square wave at the modulation frequency whose amplitude is $\frac{\Delta\bar{i}}{2}R_L$ plus a dc voltage equal to $(\bar{i}-\frac{\Delta\bar{i}}{2})R_L$. Here $\Delta\bar{i}$ is directly proportional to Δi if i results from the rectification of a sine wave. Note that Δi is not directly proportional to Δe but also depends on the slope of the function $i_b = f(e_b)$ where $e_b = e_{\max}$. The slope of the crystal response curve determines the gain of the crystal detector. The peak-to-peak voltage, $\Delta\bar{i}R_L$, of the square wave at the modulation frequency is directly proportional to the change in the microwave field, Δe , at the modulation frequency for the two samples if i results from the rectification of a sine wave and if the crystal gain is the same in each case. Since $\Delta e \ll e_{\max}$ the slope of the crystal response curve is essentially constant over the range covered by Δe so that the gain is a function of e_{\max} . However, e_{\max} for the two cases must be different to satisfy the constant power density distribution function requirement. Hence $\Delta\bar{i}R_L$ for the two cases would not be linear with absorber concentration.

If the maximum voltage across the crystal, $(e_b)_{\max}$, is constant for all cases the crystal gain is also constant. As discussed in Chapter I, previous investigators have simply added microwave radiation to the radiation that has traversed the absorbing medium to achieve this condition. For the two

cases in Figure 5, one would simply add to the radiation that has traversed the cell with sample B microwave radiation of the same frequency and phase whose amplitude is $(e_A)_{\max} - (e_B)_{\max}$ so that the resulting $(e_b)_{\max}$ is the same for both cases. This is usually accomplished via a microwave bridge arrangement.

In this research an electronic method for maintaining a constant $(e_b)_{\max}$ is employed. From Figure 5 it is evident that if a reverse bias voltage equal to $(e_A)_{\max} - (e_B)_{\max}$ is applied to the crystal in case A, $(e_b)_{\max}$ will be the same for both cases. This voltage is applied and monitored by the crystal current control device depicted schematically in Figure 6. The ac and dc signals are separated by the choke and capacitor shown in the figure. The ac signal then becomes the input to the Good preamp. The dc current can be measured by the meter in the battery-out position or it can be adjusted with the potentiometer in the battery-in position. The capacitor is included in the battery branch so that the impedance for the modulation signal remains essentially constant for both switch positions.

The major problem in evaluating the use of the crystal current control device lies in determining the degree to which $(e_b)_{\max}$ is kept constant by keeping the meter current constant. The meter current is essentially equal to the average crystal current if the current through the load resistor is very small in comparison to the meter current. The

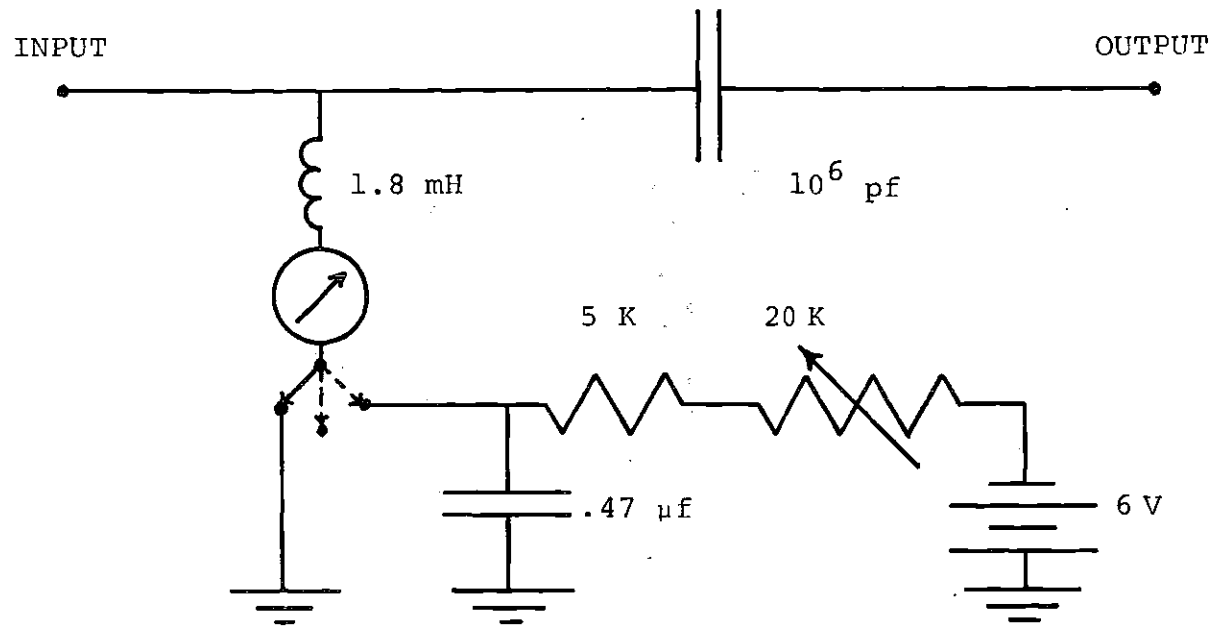


Figure 6. Crystal Current Control Device

average crystal current is equal to the maximum crystal current divided by a constant if i results from the rectification of a sine wave. If one is to monitor the maximum crystal current by the average crystal current the proportionality between them must be maintained. The average crystal current is given by

$$\bar{i}_b = \frac{1}{T} \int_{t_1}^{t_2} f(e_b) dt \quad (13)$$

where $i_b = f(e_b)$ is the crystal response function, T is the microwave period, t is the time and t_1 and t_2 are the $e = 0$ intercepts for the microwave field. Here $t_1 = 0$ and $t_2 = T/2$. If the external voltage is applied such that $\Delta(e_b)_{\max} = 0$ the voltage across the crystal will be the sum of e and a negative dc voltage as shown in Figure 7. The limits on the integral in equation (13) will change to t_1' and t_2' . From the figure one can see that if the external voltage applied such that $\Delta(e_b)_{\max} = 0$ is much smaller than the maximum value of the voltage induced in the probe, e_{\max} , the limits on the integral in equation (13) will remain essentially the same. If this condition is satisfied and if the meter current is equal to the average crystal current the maximum crystal bias voltage can be kept constant to a good approximation by keeping the meter current constant.

An experimental test was conducted to show that the

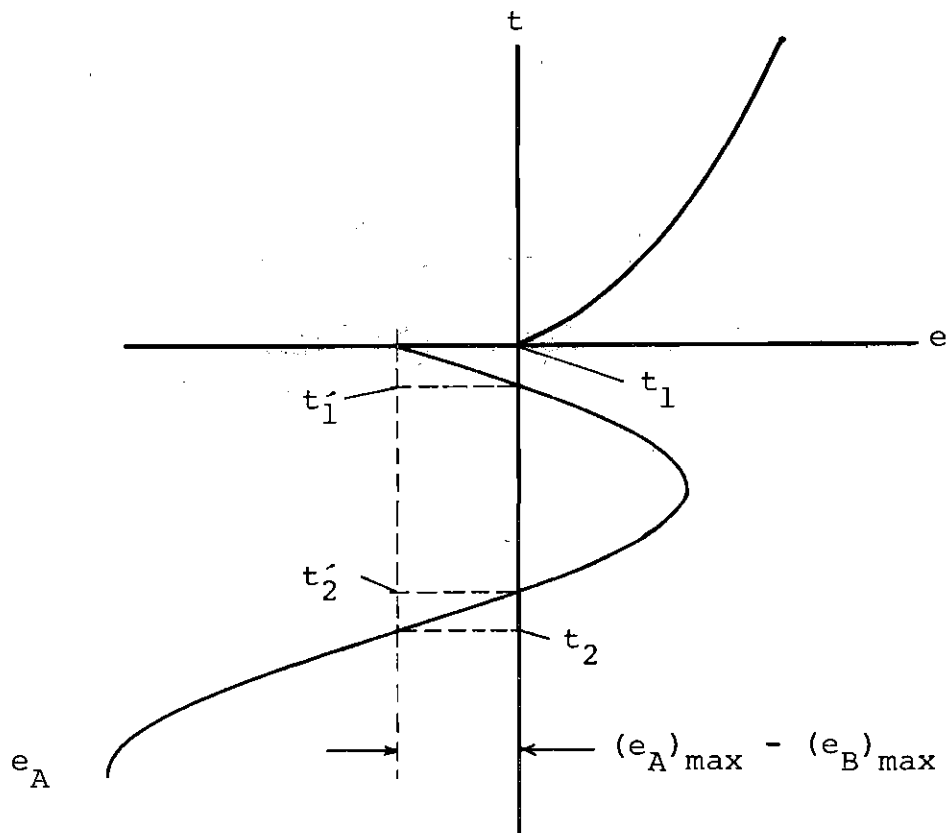


Figure 7. Crystal Input Waveform as a Result of External Applied Voltage

above conditions are satisfied over the entire range of sulfur dioxide partial pressures involved in the construction of the calibration curve. Two samples having partial pressures of SO_2 near the two extremes were prepared and the MRR lines were displayed and maximized by the procedure set forth in Chapter III. The average meter current was adjusted to one milliamp in each case. The voltage across the 6.2K load resistor was measured and recorded allowing the calculation of the average current through it. By inspection of the circuit diagram it is evident that the voltage across the load resistor is the amount the e waveforms are shifted to the left with respect to the crystal response curve. The average crystal current is just the meter current minus the current through the load resistor. From the average crystal current and a crystal response curve e_{max} can be calculated by assuming the crystal current results from the positive portion of the sine wave so that $e_{max} = \pi e_{avg}$. The measured values for the voltage across the load resistor, the meter current, the signal $S(v)$, the partial pressures of SO_2 , the total sample pressures, the calculated values for e_{max} , the current through R_L , and the average crystal current are recorded in Table 2. The resulting waveforms are depicted in Figure 8. It is evident that e_{max} is much greater than V_L so that the average crystal current can be used to maintain a constant $(e_b)_{max}$ throughout the entire range of partial pressures of SO_2 used in this research. Furthermore, the average meter

Table 2. Experimental Data Supporting the Effectiveness of the Crystal Current Control Device

	Sample A	Sample B
$P_{(SO_2)}$	30 millitorr	3 millitorr
V_L	0.16 V	0.04 V
I	1 mA	1 mA
P_T	100.9 millitorr	100.2 millitorr
e_{max}	1.20 V	1.36 V
I_L (mA)	0.025	0.006
S (v)	69.3 μ v	8.3 μ v
\bar{i}_b	0.975 mA	1.0 mA

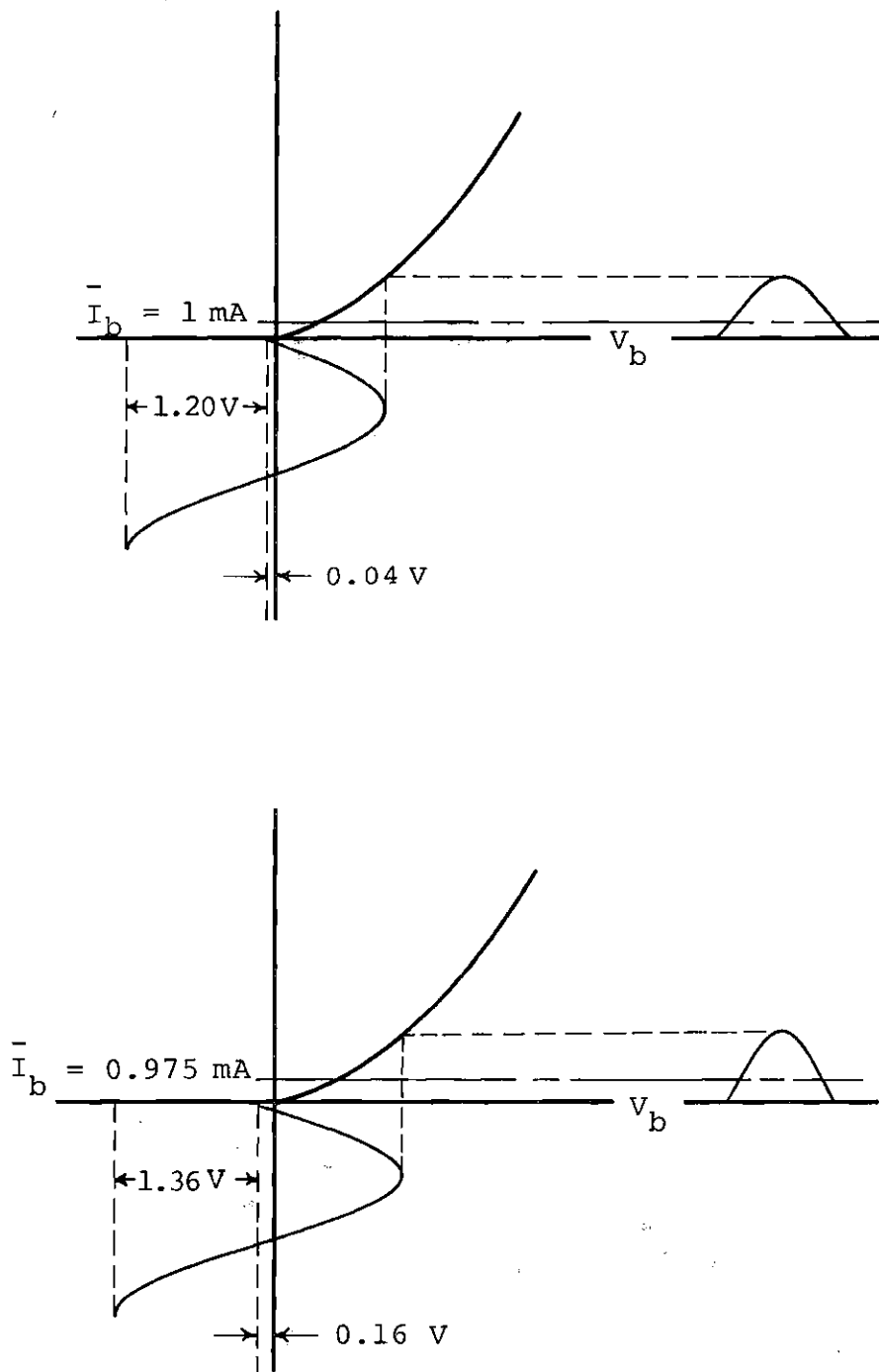


Figure 8. Crystal Detector Waveforms for SO_2 Using the Crystal Current Control Device

current can be used to maintain the constancy of the average crystal current since they are essentially equal.

CHAPTER III

CALIBRATION PROCEDURE

In order to deduce absorber concentrations from absolute MRR line intensity measurements it is necessary to measure the incident microwave power and the change in the microwave power resulting from absorption by the gas. The incident power is easily measured but in order to relate the signal out of the crystal detector to the change in power at the probe the overall crystal detector gain must be determined. To circumvent this problem other investigators have used a calibration arm that provides 100% Stark frequency modulated microwave radiation of known amplitude that is combined in phase with the radiation that has traversed the cell (24, 25) and 180° out of phase with sample absorption. When this radiations amplitude is exactly the same size as the change in amplitude of the radiation traversing the cell, no signal will be observed at the Stark modulation frequency. This null allows one to deduce the change in power resulting from absorption in the cell by making precision attenuation measurements in the calibration arm. Instead of trying to duplicate this procedure it was decided in this research to construct a calibration curve from which one could deduce the partial pressure of a species of gas in the Stark cell from a measurement of the MRR line intensity by the procedure set

forth in this chapter. In order to construct a calibration curve one simply introduces samples of known composition into the Stark cell and measures the MRR line intensity under the same set of conditions for each sample.

Sample Preparation

The most obvious method of obtaining samples of known composition is to purchase commercial samples. This may be acceptable where few samples are needed but as one needs many samples to construct a calibration curve it is desirable to have the capability to prepare samples of any composition built into the apparatus. The capability to prepare samples in the absorption cell requires only that the pure constituent gasses be available and that some means be employed by which these samples may be introduced into the cell and mixed in varying quantities while maintaining a constant total pressure. The gas handling system described in Chapter II has this capability.

The method chosen to prepare the samples is the pressure ratio method. In the pressure ratio method the sample gas is leaked into the system to the desired partial pressure P_S as measured by the Baratron. The mixer gas is then leaked in to bring the total pressure up to the desired value P_T , and the two gases are allowed to mix. In order to prepare another sample, part of the mixer sample in the cell is pumped out leaving a total pressure of P'_T in the system.

Mixer gas is then leaked in to bring the total pressure back to P_T . The mixture is considered to be homogeneous so the new partial pressure of the sample gas is proportional to the ratio of P'_T to P_T . We have the following equation

$$P'_S = P_S \frac{P'_T}{P_T} \quad (15)$$

where P'_S is the new sample partial pressure.

It is necessary to determine the amount of time needed for the two gases to mix thoroughly. To this end one may make a sample and observe the spectrometer response as a function of time. This was done with a sample containing 30.88 millitorr of SO_2 in a total pressure of 100.26 millitorr (SO_2 and N_2) and the results are shown in Figure 9. Based on these results a mixing time of fifteen minutes was selected. Once the sample is prepared and given time to mix thoroughly the spectrometer response can be measured.

MRR Line Intensity Measurement

According to the theory the height of the maximum line peak is directly proportional to the absorber concentration. Other investigators have locked the klystron to the frequency for peak absorption and used the voltage deflection of the lock-in detector as the measurement of the line intensity. Small changes in klystron power supply voltages may shift the klystron frequency and thus cause significant errors in

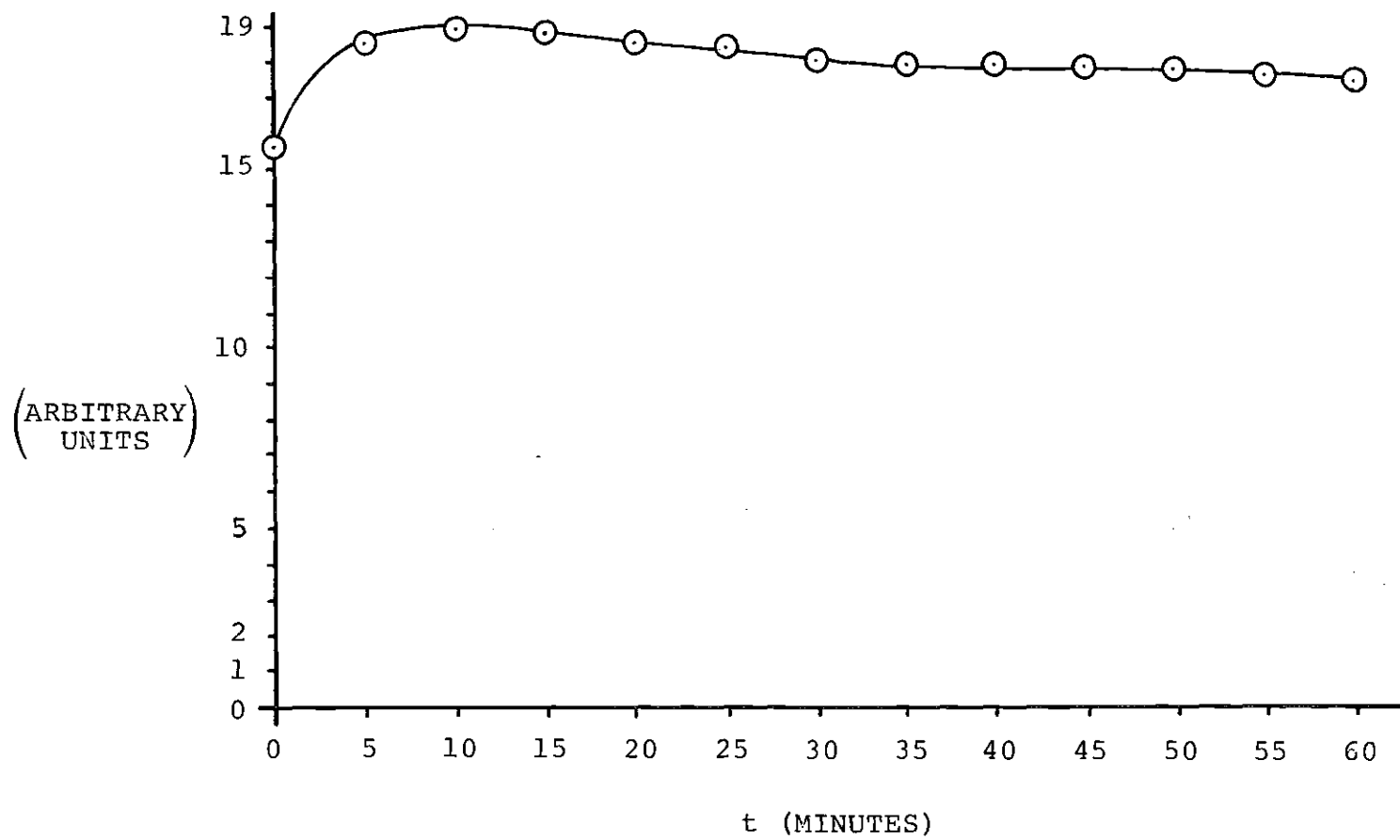


Figure 9. Signal Stabilizes Within Fifteen Minutes

intensity data. It was decided to electronically sweep the klystron through a band of frequencies thus displaying the MRR line and its Stark component on the face of the oscilloscope. In measuring the line intensity from such a display some ambiguity in the baseline exists. The line may also be subject to interference from the Stark lobe if the Stark voltage is not great enough. To alleviate these problems it was decided to use the MRR line peak to Stark lobe peak voltage at constant Stark voltage as the measure of spectrometer response $S(v)$. This is possible because the Stark peak appears as a negative or downward deflection of the beam on the trace. If the absorption frequency is not on the flat part of the klystron mode the oscilloscope trace will not be horizontal. If this is the case one should display the mode on the scope and adjust the klystron reflector voltage and the micrometer screw on the klystron so that the frequency meter pip at the absorption frequency is on the flat part of the mode.

Before measuring the MRR line intensity experimental conditions discussed in Chapter I must be satisfied. This is achieved by adopting the following procedure. Using the variable microwave attenuator adjust the power so as to maximize the signal, $S(v)$. Switch the crystal current control device to the battery-in position and adjust the current to the desired value. Remaximize the line with the microwave attenuator and select an Eductor time constant to enhance the

signal to noise ratio without reducing the signal. This step may be necessary before maximizing the line. Read and record the peak-to-peak voltage, $S(v)$, directly from the oscilloscope. Record the PAR lock-in sensitivity and the Eductor gain. Proceed to prepare another sample if desired.

CHAPTER IV

THE CALIBRATION CURVE

According to Harrington's theory the maximum microwave spectrometer response is linear with the concentration of the absorbing gas in the Stark cell and hence its partial pressure. In this research a calibration curve was constructed to allow one to deduce the partial pressure of sulfur dioxide in a sample whose total pressure was one hundred millitorr via a measurement of the maximum Stark peak to MRR line peak voltage of the 9403.22 MHz line (26) for partial pressures of SO_2 in the range of one to thirty millitorr. The calibration curve was constructed, using a Stark voltage of 500 volts, a klystron power supply beam current of 65 milliamps, and a direct current through the crystal current control device meter equal to one milliamp, and these conditions must be used when making measurements on unknowns. As previously noted the samples were prepared via the pressure ratio method, and the line intensity was then measured following the procedure outlined in Chapter III. Samples covering the entire range of sulfur dioxide partial pressures were prepared by letting in approximately thirty millitorr of SO_2 for the initial sample, bringing the total pressure up to one hundred millitorr with nitrogen, and preparing the remaining samples in the sequence via the pressure ratio method. The factor

that distinguishes one sequence of samples is the P'_T associated with the sample preparation. The larger the P'_T the larger the number of samples prepared in covering the entire range of partial pressures involved and hence the more time required.

The experimental data and the best straight line as determined by the least squares fit computer program (see Appendix A) are presented in Figure 10. The points associated with each test run and the corresponding P'_T are coded and can be distinguished by referring to the legend in the lower right hand corner of the figure. The error bar in the figure represents the error in reading the signal from the oscilloscope trace as a result of noise not eliminated by the detection apparatus. The raw experimental data used to construct the calibration curve, sample calculations, and a copy of the computer printout are included in Appendix B. The functional form of the calibration curve is

$$S(\mu v) = (1.41 \pm 0.54) + (2.37 \pm 0.18)P$$

where $S(\mu v)$ is the signal in microvolts in terms of the peak-to-peak voltage out of the crystal detector, and P is the partial pressure of sulfur dioxide in millitorr of mercury. To facilitate the inspection of the data, slope-intercept and corresponding error values are presented in Table 3 for each of the four test runs.

The major indication of the calibration curve and the

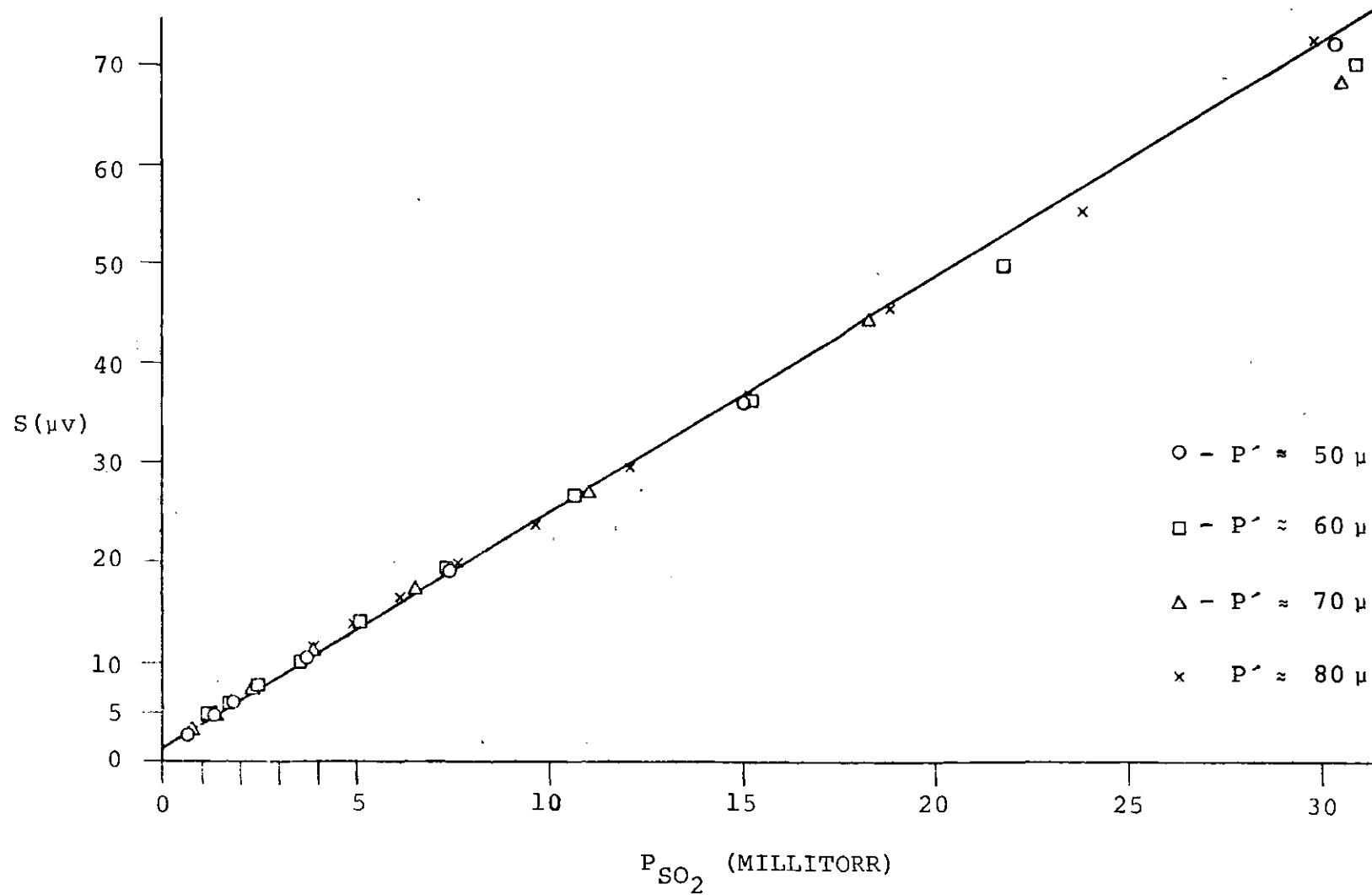


Figure 10. The Calibration Curve

Table 3. Slope Intercept Data for the Calibration Curve and the Four Test Sequences

P_T' (millitorr Hg)	Slope ($\mu\text{V}/\text{millitorr}$)	Intercept (μV)
50	2.41 ± 0.13	1.14 ± 0.26
60	2.36 ± 0.16	1.34 ± 0.39
70	2.28 ± 0.12	2.14 ± 0.42
80	2.23 ± 0.05	2.83 ± 0.45
TOTAL	2.37 ± 0.18	1.41 ± 0.54

associated computer output is that the microwave line intensity is a linear function of the partial pressure of sulfur dioxide within an error of 7.6 per cent if the requirements on the experimental conditions mentioned above are strictly observed. One may also determine the maximum sensitivity of the instrument from these findings. The noise level for the spectrometer oscilloscope trace was $0.13 \mu\text{v}$. Assuming that the minimum detectable change in signal is two times the noise one can calculate the minimum change in partial pressure of SO_2 as follows. Assuming $S = 0.26$ we have

$$0.26 \mu\text{v} = 2.37 \Delta P_{\text{min}}$$

so

$$\Delta P_{\text{min}} = 0.1 \text{ millitorr.}$$

The minimum detectable change in sulfur dioxide content is 0.1 millitorr.

Note that in Table 3 the factor that distinguishes one set of data from the others is the P_T' associated with the measurement sequence. The greater the P_T' involved in the sequence the greater the number of data points required to cover the entire range of partial pressures investigated. As a result more time elapses in the sequence with the larger P_T' . A close study of Table 3 reveals that the slope of the calibration curve for each individual sequence decreases and the corresponding intercept value increases as more time is

needed to complete the sequence. This suggests that some time-dependent mechanism is responsible for the alteration of the sample. Three likely possibilities are discussed below.

If the pumping efficiency is different from the nitrogen and sulfur dioxide such that nitrogen is pumped out at a slightly greater rate the result would be a greater concentration of sulfur dioxide present in the absorption cell than calculated via the pressure ratio method. Each time the cell must be pumped to prepare a sample the effect would be compounded. Thus differential pumping would decrease the slope and increase the intercept to a degree determined by the number of experimental events necessary to complete the sequence.

Suppose that during the initial introduction of sulfur dioxide into the system a quantity thereof is adsorbed on the walls of the cell and gas handling system or foreign material contained therein and eventually equilibrium is established between the adsorbed gas and the gas present in the cell. Once the cell is pumped to prepare a new sample the equilibrium would no longer exist. A new equilibrium would be established by outgassing of the adsorbed sulfur dioxide. The result, again, would be a greater concentration of sulfur dioxide than that calculated, compounded to a degree determined by the number of experimental events necessary to cover the sequence.

Lastly, the method used to mix the gases, that is, merely by their thermal velocities, compounded by the geometry of the gas handling system and absorption cell may result in concentration gradients in the systems. These gradients could result in a greater concentration of sulfur dioxide in the absorption cell, and the effect would be compounded by the preparation of subsequent samples.

The above mechanisms are discussed as possible means by which the curious nature of the data contained in Table 2 can be explained. However, on the basis of this research it is not possible to determine which, if any, is responsible for the trend in the data.

CHAPTER V

CONCLUSIONS AND RECOMMENDATIONS

The dependence of the Stark component peak to the microwave line peak voltage, $S(\mu\text{v})$, of the 9403.22 MHz line on the partial pressure of sulfur dioxide within the absorption cell is given by the following equation

$$S(\mu\text{v}) = (1.41 \pm 0.54) + (2.37 \pm 0.18)P$$

The linearity of the peak to peak voltage to the partial pressure is thus determined to be within 7.6 per cent. The maximum sensitivity, that is the minimum detectable change in the partial pressure of sulfur dioxide in the cell as calculated is 0.1 millitorr. The slope-intercept data for individual test runs indicates that as the number of experimental events necessary to cover the total range of partial pressures increases the slope decreases, and the intercept increases. This strongly suggests that the sample undergoes some alteration during the process of taking the data. It was not possible to deduce the exact nature of this alteration.

Provided that further experimental enquiry is forthcoming utilizing the crystal current control device as a means to establish a constant crystal gain, several things are recommended. During the process of adjusting the direct

crystal current, it was noted that the Kings Electronics Co., Inc. meter display did not provide for sufficient accuracy in maintaining a direct crystal current of one milliamp. As a result it is recommended that a meter with a large, mirrored readout face be used.

As discussed in Chapter II some error is introduced into the process of maintaining a constant crystal gain by adjusting the direct crystal current to one milliamp as a result of the base-line shift of the input sine waves (see Figure 9). Actually it is the maximum crystal current one desires to keep constant. The average crystal current necessary to maintain a constant maximum crystal current is not always one milliamp but is a function of the shift in the baseline voltage. Hence it is recommended that in further research the functional dependence of the average crystal current on the baseline shift in voltage be calculated or plotted and used to more effectively maintain a constant maximum crystal current and consequently a constant crystal gain with hopes of reducing the error in the slope of the calibration curve and eliminating the intercept.

As noted in the conclusions the samples apparently undergo some alteration during the procedure of constructing the calibration curve. The error associated with this alteration is compounded each time a new sample is prepared. As an alternative to this method of sample preparation a dynamic method is recommended. In such a method the gases would be

mixed at relatively high pressures in a chamber outside the absorption cell which is continuously pumped. The mixture would then be leaked through the cell and the cell total pressure could be maintained at a lower level than 100 millitorr. For any new sample a steady state condition would soon be effected for adsorption and outgassing so that the composition of each sample would not be affected. Since the gases would be mixed outside of the cell mechanical means could be employed to assure a homogeneous mixture. With the total pressure at a lower level the MRR line would undergo less collision broadening and hence would result in greater sensitivity of the spectrometer.

APPENDIX A

A least squares fit computer program was used to find the slope and intercept of the best straight line for the data. The computer program assumes that the functional form of the relationship for each experimental event i is

$$S_i - \epsilon_i = a_1 + a_2 P_i$$

where S_i is the spectrometer response, ϵ_i is the error, P_i is the partial pressure of sulfur dioxide in the Stark cell, a_1 is the $P_i = 0$ intercept, and a_2 is the slope of the straight line. a_1 and a_2 are determined by varying them until the variance defined by the equation

$$\sigma = \sum_i \frac{[S_i - \epsilon_i - (a_1 + a_2 P_i)]^2}{S_i}$$

is minimized. This achieved by simultaneously requiring that $\frac{\partial \sigma}{\partial a_1} = 0$ and $\frac{\partial \sigma}{\partial a_2} = 0$. The program also gives an estimation in the error, a_1' and a_2' , associated with a_1 and a_2 . The error can be shown to be for a_1

$$a_1' = \left[\frac{\sigma \sum_i \frac{P_i^2}{S_i^2}}{\sum_i \frac{P_i^2}{S_i^2} - \left(\sum_i \frac{P_i}{S_i} \right)^2} \right]^{\frac{1}{2}}$$

and for a_2

$$a_2' = \left[\frac{\sigma}{\sum_i \frac{P_i^2}{S_i^2} - \sum_i \frac{P_i}{S_i}} \right]^{\frac{1}{2}}$$

The final functional forms of the equation is as follows.

$$S = (a_1 \pm a_1') + (a_2 \pm a_2')P$$

APPENDIX B

The data was taken in four different sequences as previously discussed. The data was recorded in the following manner. After the cell had been pumped overnight SO_2 was introduced to bring the pressure up to roughly thirty millitorr. The pressure was allowed to stabilize and the precise pressure was read and recorded along with the time. Nitrogen was leaked in to bring the total pressure to roughly 100 millitorr. After stabilization the pressure was measured and recorded with the time. The gases were then given roughly 15 minutes to mix, after which the line was maximized, the crystal current adjusted to 1 mA, and the signal $S(v)$, the PAR sensitivity, the Eductor gain, the total pressure, and the time were recorded. The cell was then pumped to bring the total pressure down to P'_T . The pressure was allowed to stabilize and was recorded with the time. Nitrogen was leaked in to bring the total pressure back to roughly 100 millitorr. Once the pressure stabilized it was recorded with the time. The new sample was allowed to mix thus repeating the process above. The new pressure of SO_2 was calculated by using the total pressure after the gases were allowed to mix. Taking the data from Table 4 for the first mixture we have

$$P'_S = 30.42 \left(\frac{49.46}{99.96} \right) \text{millitorr} = 15.05 \text{ millitorr.}$$

The calculated new partial pressure is also recorded. In Table 7 the signals with and without the Good preamp in the circuit are recorded for each sample and the gain is calculated in the following manner:

$$G = \frac{S_{\text{with}}}{S_{\text{without}}} = \frac{19.0\text{v}}{1.39\text{v}} = 13.67$$

The gain for each sample is recorded and the average of these is used to calculate the signal, $S(\mu\text{v})$, out of the crystal detector in the following manner:

$$S(\mu\text{v}) = S(\text{v}) \times \frac{1}{G_E} \times \frac{1}{\text{PAR Sensitivity}} \times \frac{1}{G_{\text{Good}}}$$

For the first sample we have

$$\begin{aligned} S(\mu\text{v}) &= 19.5\text{v} \times \frac{1}{1} \times \frac{1}{1\text{v}/500\mu\text{v}} \times \frac{1}{13.52} \\ &= 72.12 \mu\text{v} \end{aligned}$$

The calculated signal, $S(\mu\text{v})$, out of the crystal detector is also recorded in the tables below. Following the tables is a copy of the computer printout.

Table 4. Test Sequence One

P_{SO_2}	P_T	P'_T	S (v)	PAR	G_E	S (μ v)	t
30.42	99.26 99.98	49.46	19.5	500	1	72.12	4:27
15.05	99.97 100.00						
7.46	100.57 100.49	49.54	25.8	500	5	19.08	5:17
3.72	100.22 100.08	50.15					
1.87	133.62 133.43	50.19	8.0	500	5	10.5	5:45
1.38	98.88 98.81	98.88					
0.70	100.20 99.98	49.75	15.6	200	5	4.62	6:11
			9.1	200	5	2.69	

Table 5. Test Sequence Two

P_{SO_2}	P_T	P'_T	S (v)	PAR	G_E	S (μ v)	t
30.55							4:36
	100.25						4:41
	99.79		18.5	500	1	68.42	5:00
		60.12					5:05
18.32	99.78						5:08
	99.74		12.0	500	1	44.38	5:23
		60.19					5:28
11.05	99.94						5:32
	100.00		14.6	500	2	27.00	5:48
		59.20					5:54
6.55	100.02						5:58
	100.15		9.4	500	2	17.38	6:14
		59.53					6:21
3.90	100.16						6:24
	100.34		15.1	500	5	11.17	6:45
		59.58					6:50
2.32	100.12						6:55
	100.32		24.7	200	5	7.31	7:12
		60.05					7:16
1.39	105.05						7:19
	105.22		15.8	200	5	4.67	7:35
		60.25					7:39
0.80	99.92						7:43
	100.17		10.4	200	5	3.08	8:02

Table 6. Test Sequence Three

P_{SO_2}	P_T	P'_T	S (v)	PAR	G_E	S (μ v)	t
30.93							10:12
	99.94						10:16
	99.28		19.0	500	1	70.27	10:31
		70.00					10:36
21.81	100.08						10:39
	99.88		13.5	500	1	49.93	10:52
		69.82					10:57
15.24	100.00						11:00
	99.92		9.80	500	1	36.24	11:15
		69.82					11:20
10.65	99.94						11:23
	99.97		7.22	500	1	26.70	11:40
		69.26					11:44
7.38	101.30						11:46
	101.37		10.5	500	2	19.42	12:01
		70.09					12:06
5.10	100.04						12:09
	100.15		7.64	500	2	14.13	12:25
		69.55					12:32
3.55	101.08						12:35
	101.19		5.96	500	2	11.02	12:51
		69.84					12:56
2.45	100.09						12:59
	100.26		4.20	500	2	7.77	1:16
		70.04					1:21
1.71	101.86						1:24
	102.04		8.10	500	5	5.99	1:43
		69.00					1:47
1.16	100.16						1:50
	100.37		6.22	500	5	4.60	2:06

NO RUN ACTIVE

@RUN PHRAP, 011R0635, STEPHENS-M-A, S15

DATE: 09/18/73 TIME: 21:27:23 LINE: 4364

@XOT PAT.

SPD C, NE, IX, X, Y, Z, LX

SPD NE=35, X=30.42, 15.05, 7.46, 3.72, 1.87, 1.38, .7, 30.55, 18.32,
11.05, 6.55, 3.9, 2.32, 1.39, .8, 30.93, 21.81, 15.24, 10.65, 7.38, 5.1,
3.55, 2.45, 1.71, 1.16, 29.86, 23.86, 18.9, 15.16, 1.2, 2.1, 9.64, 7.68,
6.16, 4.91, 3.92, Y=72.12, 36.24, 19.08, 10.5, 5.92, 4.62, 2.69, 68.42,
44.38, 27, 17.38, 11.17, 7.31, 4.67, 3.08, 70.27, 49.93, 36.24, 26.7,
19.42, 14.13, 11.02, 7.77, 5.99, 4.60, 70.27, 55.47, 45.49, 36.98, 29.59,
23.89, 19.97, 16.27, 13.9, 11.69, LX=1, SEND

I	PAR	FRP
1	.1412+01	.5407+00
2	.2370+01	.1810+00

INPUT DATA

1	.3042+02	.7212+02	.1000+01
2	.1505+02	.3624+02	.1000+01
3	.7460+01	.1908+02	.1000+01
4	.3720+01	.1050+02	.1000+01
5	.1870+01	.5920+01	.1000+01
6	.1380+01	.4620+01	.1000+01
7	.7000+00	.2690+01	.1000+01
8	.3055+02	.6842+02	.1000+01
9	.1832+02	.4438+02	.1000+01
10	.1105+02	.2700+02	.1000+01
11	.6550+01	.1738+02	.1000+01
12	.3900+01	.1117+02	.1000+01
13	.2320+01	.7310+01	.1000+01
14	.1390+01	.4670+01	.1000+01
15	.8000+00	.3080+01	.1000+01
16	.3093+02	.7027+02	.1000+01
17	.2181+02	.4993+02	.1000+01
18	.1524+02	.3624+02	.1000+01
19	.1065+02	.2670+02	.1000+01
20	.7380+01	.1942+02	.1000+01
21	.5100+01	.1413+02	.1000+01
22	.3550+01	.1102+02	.1000+01
23	.2450+01	.7770+01	.1000+01
24	.1710+01	.5990+01	.1000+01
25	.1160+01	.4600+01	.1000+01
26	.2986+02	.7027+02	.1000+01
27	.2386+02	.5547+02	.1000+01

28	.1890+02	.4549+02	.1000+01
29	.1516+02	.3698+02	.1000+01
30	.1210+02	.2959+02	.1000+01
31	.9640+01	.2389+02	.1000+01
32	.7680+01	.1997+02	.1000+01
33	.6160+01	.1627+02	.1000+01
34	.4910+01	.1390+02	.1000+01
35	.3920+01	.1169+02	.1000+01

SRD C,NE,IX,X,Y,Z,LX
 SRD Z(1)=35*0,Z(1)=7*1,SEND

I	PAR	ERR
1	.1135+01	.2641+00
2	.2408+01	.1335+00

SRD C,NE,IX,X,Y,Z,LX
 SRD Z(1)=7*0,Z(8)=8*1,SEND

I	PAR	ERR
1	.1342+01	.3889+00
2	.2363+01	.1619+00

SRD C,NE,IX,X,Y,Z,LX
 SRD Z(8)=8*0,Z(16)=10*1,SEND

I	PAR	ERR
1	.2135+01	.4280+00
2	.2277+01	.1227+00

SRD C,NE,IX,X,Y,Z,LX
 SRD Z(16)=10*0,Z(26)=10*1,SEND

I	PAR	ERR
1	.2832+01	.4491+00
2	.2229+01	.5494-01

SRD C,NE,IX,X,Y,Z,LX
 @EOF
 END 506 MLSEC
 @FIN

BIBLIOGRAPHY

1. James P. Tomany, Air Pollution, The Emissions, The Regulations, and the Controls (American Elsevier Publishing Co., Inc., New York, 1975), p. 4.
2. Thomas H. Maugh II, Science, 177, 685-687, (1972).
3. John R. Hearn, Wescon Technical Papers, 32/4, (1971).
4. W. F. White, Chemical Engineering Progress Symposium Series, #63, Vol. 62, (1966).
5. R. D. Mattuck and M. W. P. Strandberg, Review of Scientific Instruments, 29, 717-721 (1958).
6. P. H. Verdier and E. B. Wilson, Journal of Chemical Physics, 29, 340-347 (1958).
7. A. S. Esbitt and E. B. Wilson, Jr., Review of Scientific Instruments, 34, 901-907 (1963).
8. B. P. Dailey, Analytical Chemistry, 21, 540-544 (1949).
9. William H. Kirchhoff, Chemical and Engineering News, Vol. 47, Part 1, 88-98 (1969).
10. Gordon E. Jones and Everette T. Beers, Analytical Chemistry, Vol. 43, No. 6, 656-659 (1971).
11. Lawrence W. Hrubesh, AIAA Paper No. 71-1048 (1971).
12. C. H. Townes and A. L. Schawlow, Microwave Spectroscopy (McGraw-Hill Book Co., Inc., New York, 1955), p. 371.
13. Ibid., 492-497.
14. Ibid., 371-373.
15. Howard W. Harrington, Journal of Chemical Physics, Vol. 46, No. 10, 3698-3707 (1967).
16. Howard W. Harrington, Journal of Chemical Physics, Vol. 49, No. 7, 3023-3035 (1968).
17. Ibid., 3023-3025.

18. Ibid., 3025-3029.
19. Howard W. Harrington, Journal of Chemical Physics, Vol. 46, No. 10, 3698-3707 (1967).
20. W. E. Good, Scientific Paper, 1538 Westinghouse Research Laboratories.
21. Matheson Gas Products General Catalog, 83 and 72 (1973).
22. Operating Note, Hewlett-Packard Co., No. 00240-4, p. 3.
23. Howard W. Harrington, Journal of Chemical Physics, Vol. 46, No. 10, 3698-3707 (1967).
24. Howard W. Harrington, Journal of Chemical Physics, Vol. 44, 3481 (1966).
25. R. F. Curl, Jr., Journal of Molecular Spectroscopy, Vol. 29, 375-383 (1969).
26. Howard W. Harrington, Journal of Chemical Physics, Vol. 49, No. 7, 3025 (1968).